PAPER

Check for updates

Multiscale porous single-atom Co catalysts for epoxidation with O₂†

Xiao Chen,‡[ab] Yong Zou,‡[ac] Mingkai Zhang,[c] Wangyan Gou,[a] Sai Zhang ⑮ *[a] and Yongquan Qu*[ac]

Epoxides are versatile intermediates in the production of a diverse set of chemical products. The direct epoxidation of alkenes using O₂ represents an environmentally friendly and economical process to replace the use of expensive H₂O₂ or organic peroxides for the synthesis of epoxides. Herein, single-atom Co anchored on N-doped carbon supports with a multiscale porous structure (Co₁/NC-h) has been successfully constructed by etching CoZn-ZIF metal–organic framework precursors before a carbonation process. Benefitting from the high intrinsic activity of Co–Nₓ active sites and the more accessibly exposed reactive sites of multiscale porous structures, the Co₁/NC-h catalysts can achieve the epoxidation of cyclooctene with 95% yield of 1,2-epoxycycloheptane at 140 °C and 0.5 MPa O₂. This research opens up opportunities for designing high-performance single-atom catalysts towards applications in diverse heterogeneous catalysis.

Introduction

Alkene epoxidation is an important fundamental and industrially applicable chemical process to yield epoxides, which are versatile intermediates with an annual production of multi-million tons from a wide range of synthetic routes.[1–4] Generally, hydrogen peroxides (H₂O₂, *tert*-butyl hydroperoxide, *etc.*) are used as terminal oxidants to achieve alkene epoxidation with various homogeneous and heterogeneous transition metal catalysts.[5–10] However, the extensive use of peroxides inevitably leads to an increase in the costs. As a result, the direct selective formation of epoxides using O₂ is a cost-effective and environmentally friendly strategy.[11,12] However, this ideal process is still challenging with respect to both activity and selectivity. Recently, various polyoxometalates, transition metal compounds, and Au-based heterogeneous catalysts have been developed to achieve alkene epoxidation.[13–19] Unfortunately, these catalytic systems have not been verified in industrial applications. Also, only the epoxidation of ethylene can be realized using O₂.[20] Therefore, to find efficient heterogeneous

catalysts which could be suitable for practical applications is of great significance.

Owing to the unique atom utilization and satisfactory selectivity, the application of single-atom catalysts has received growing attention.[21,22] Lately, carbon-based materials have been proven to be an enormous family of single-atom catalysts because of their specific features including superb chemical and mechanical stability, high specifical surface properties and area, low production cost, easy handling, and so on.[23–26] Inspired by their behaviours in catalysing peroxide activation and efficiencies in advanced oxidation processes, carbon-based single-atom catalysts provide a promising opportunity for efficiently activating O₂ for alkene epoxidation. Particularly, transition metal (M)–nitrogen carbon materials with atomically dispersed M–Nₓ active sites are considered as the most encouraging breakthrough case owing to their widely proven capacity to effectively active O₂ in various oxygen reduction reactions.[27–30] Generally, metal–organic frameworks (MOFs) as precursors with specific morphologies can assist the preparation of carbon-based single-atom catalysts *via* a carbonization process at high temperature (>700 °C).[31–33] However, the internal diffusion of reactants in these catalysts is inevitably weakened by the narrow passage in heterogeneous catalysis. As a result, only <10% of the M–Nₓ sites in carbon-based single-atom catalysts are involved in catalytic reactions.[34,35] Moreover, this phenomenon is further exacerbated in liquid heterogeneous catalysis with relatively large reactant molecules. Therefore, constructing multiscale porous structures is particularly desirable for carbon-based single-atom catalysts to achieve the efficient utilization of the M–Nₓ moieties, consequently resulting in the improvement of their catalytic ability.

ᵃKey Laboratory of Special Functional and Smart Polymer Materials of Ministry of Industry and Information Technology, School of Chemistry and Chemical Engineering, Northwestern Polytechnical University, Xi'an 710072, China. E-mail: zhangsai1112@nwpu.edu.cn; yongquan@nwpu.edu.cn

ᵇSchool of Materials Science and Engineering, North China University of Water Resources and Electric Power, Zhengzhou 450045, China

ᶜFrontier Institute of Science and Technology, Xi'an Jiaotong University, Xi'an, 710049, China

† Electronic supplementary information (ESI) available. See DOI: 10.1039/d1ta09227h

‡ These authors contributed equally to this work.

Scheme 1 Schematic diagram of the preparation of the Co_1/NC and Co_1/NC-h catalysts.

Herein, single-atom Co anchored on nitrogen-doped multi-scale porous carbon (Co_1/NC-h) with more exposed active sites has been successfully prepared to achieve high intrinsic activity for alkene epoxidation with O_2. The multiscale porous structure was constructed by etching CoZn-ZIF MOF precursors before the carbonation process. For cyclooctene epoxidation, Co_1/NC-h catalysts with a multiscale porous structure obtained a 95% yield of 1,2-epoxycycloheptane at 140 °C and 0.5 MPa O_2. Mechanism studies revealed that the $Co–N_x$ active sites exhibited a high intrinsic activity for epoxidation, while the constructed multiscale porous structure could facilitate the exposure of more $Co–N_x$ sites in the multiscale pores of catalysts. Therefore, the catalytic activity of Co_1/NC-h was greatly improved.

Results and discussion

Preparation of the Co_1/NC-h and Co_1/NC catalysts

The single-atom Co_1/NC catalysts were synthesized according to previous reports.[36–39] Initially, CoZn-ZIF with a 1 : 1 molar ratio of Co : Zn (Fig. S1, S2a and b†) were obtained as a precursor,

which could assist the formation of commonly used single-atom Co_1/NC catalysts. Then, the preparation process of single-atom Co_1/NC-h catalysts was modified with a pre-etching process of CoZn-ZIF precursors as shown in Scheme 1. For a typical etching process, the CoZn-ZIF precursors were re-dispersed in DMF and then treated at 140 °C to yield the CoZn-ZIF-h precursors. Determined by inductively coupled plasma mass spectrometry, the concentrations of free Co^{2+} and Zn^{2+} ions in the DMF solution were 5.0 and 10.0 mg L^{-1} after 24 h etching, respectively, revealing that the CoZn-ZIF precursors were partially dissolved under the treatment conditions. The rough surface of CoZn-ZIF-h further indicated the creation of large macropores in the treated ZIF in comparison with the smooth surface of the fresh CoZn-ZIF (Fig. S2c and d†). Notably, the phase of the treated CoZn-ZIF was well preserved during the etching process (Fig. S1†). Thus, the phase and coordination environment of Co were unalternated in CoZn-ZIF-h. With the same carbonization, single-atom Co_1/NC-h catalysts with a multiscale porous structure were synthesized.

Then, the morphology of carbon-based single-atom catalysts was characterized by using a scanning electron microscope (SEM) and transmission electron microscope (TEM). Compared with CoZn-ZIF precursors, the as-prepared Co_1/NC catalysts retained the initial octahedral shape (Fig. 1a). Particularly, no Co nanoparticles were observed both on the surface and/or in the bulk of the Co_1/NC catalysts from the SEM (Fig. 1a) and dark field TEM images (Fig. 1b). Meanwhile, the X-ray diffraction (XRD) pattern for Co_1/NC showed no characteristic peaks of Co or cobalt oxide crystals (Fig. S3†). However, inductively coupled plasma mass spectrometry (ICP-MS) confirmed that the content of Co was 1.2 wt% in the Co_1/NC catalysts. The distribution of the Co element was well consistent with the C and N elements

Fig. 1 Characterization of catalysts. (a) SEM and (b) dark field TEM images of Co_1/NC. (c) EDS mapping of Co_1/NC. (d) HAADF-STEM image of Co_1/NC. (e) TEM and (f) HAADF-STEM images of Co_1/NC-h. TEM images of the (g) Co/NC and (h) NC catalysts.

from the energy dispersive spectroscopy (EDS) mapping analysis, revealing that the Co atom was highly distributed on the N-doped carbon supports (Fig. 1c). Meanwhile, according to the image from the aberration corrected high-angle annular dark-field scanning transmission electron microscope (HAADF-STEM), the brighter spots were assigned to the Co atoms, further exhibiting the atomic dispersion on the Co_1/NC catalysts (Fig. 1d). Therefore, single-atom Co anchored on the N-doped carbon supports could be successfully obtained via the carbonization of CoZn-ZIF.

Meanwhile, the etched CoZn-ZIF precursors with undestroyed phase were also calcined with the same process. TEM images revealed that the as-synthesized Co_1/NC-h catalysts also exhibited an approximate octahedral shape but with obvious irregular porous features (Fig. 1e), compared with the surface of Co_1/NC catalysts. Also, a relatively rough surface of Co_1/NC-h catalysts was observed from the SEM image, compared with the surface features of Co_1/NC (Fig. S4†). Thus, some macropores were formed on the Co_1/NC-h catalysts. As for Co_1/NC catalysts, the Co nanoparticles were also not revealed from the TEM image (Fig. 1e) and XRD pattern (Fig. S3†). Meanwhile, the atomically dispersed Co atom in the Co_1/NC-h catalysts could be confirmed by combining the results of HAADF-STEM (Fig. 1f). ICP-MS analysis suggested a Co percentage of 1.1 wt% in Co_1/NC-h.

The pore distribution of the Co_1/NC and Co_1/NC-h catalysts was further analyzed by the Brunauer–Emmett–Teller (BET) method. As shown in Fig. 2a, the N_2 adsorption–desorption curves revealed that the adsorption capacity of the Co_1/NC catalysts was higher at low pressure and lower at high pressure, compared with that of Co_1/NC-h. Thus, the Co_1/NC catalyst has a larger number of micropores but a smaller number of macropores than the Co_1/NC-h catalysts. Besides, the larger specific surface of Co_1/NC (766 m^2 g^{-1}) also proved that it has a larger number of micropores compared with Co_1/NC-h (613 m^2 g^{-1}). As shown in Fig. 2b, the proportion of pores lager than 2 nm was 23.8% on Co_1/NC, which was obviously smaller than that of Co_1/NC-h (45.1%). These characterization results were in accordance with the previous statement that the Co_1/NC-h catalysts exhibited a larger number of relatively large pores. In addition, the Co_1/NC-h catalysts also exhibited a reduced pore size in the range of 1–2 nm compared with the Co_1/NC catalysts (Fig. 2c).

Therefore, the increased number of macropores and the reduced number of micropores could contribute to the formation of a multiscale porous structure in the Co_1/NC-h catalysts.

Catalytic performance of cyclooctene epoxidation

The epoxidation of cyclooctene was selected as the model reaction to investigate the catalytic performance of the synthesized catalysts, and the reaction was performed in DMF solution at 140 °C and 0.5 MPa O_2. To highlight the catalytic performance of single-atom catalysts, Co nanoparticles anchored on N-doped carbon (Co/NC, Fig. 1g) and pure N-doped carbon (NC, Fig. 1h) were also prepared as referenced catalysts via the same carbonization of Co-ZIF (Fig. S5a and b†) and Zn-ZIF (Fig. S5a and c†) precursors, respectively. The Co content in Co/NC catalysts was 49.0 wt%, determined by ICP-MS analysis. Although the epoxidation of cyclooctene could occur in the DMF solution without catalysts, the reaction activity was greatly enhanced with Co-based catalysts (Fig. 3a). After 3 h of reaction, the Co_1/NC-h catalyst obtained a 58% yield of 1,2-epoxycycloheptane, which was 4.1, 4.8, 11.6 and 14.5 times higher than the yield obtained with Co_1/NC (14%), Co/NC (12%), and NC (5%) and without catalysts (4%), respectively. Obviously, the Co_1/NC-h catalysts exhibited the highest catalytic activity for the epoxidation of cyclooctene.

Meanwhile, the superior catalytic activity of single-atom Co catalysts would be further demonstrated when normalizing the reaction rate of cyclooctene epoxidation based on the total content of Co in each catalyst. As shown in Fig. 3b, the reaction ratio of Co_1/NC catalysts was 30 mmol $mmol_{Co}^{-1}$ h^{-1}, which was 63 times higher than that of Co/NC (0.48 mmol $mmol_{Co}^{-1}$ h^{-1}). Obviously, the single-atom catalysts exhibited nearly two orders of magnitude increase in catalytic activity compared with nanocatalysts. Also, the Co_1/NC-h catalysts with a multiscale porous structure exhibited a further increased reaction rate from 30 mmol $mmol_{Co}^{-1}$ h^{-1} to 106 mmol $mmol_{Co}^{-1}$ h^{-1}. Therefore, owing to the single-atom Co and the multiscale

Fig. 2 (a) Adsorption–desorption curves of N_2, (b) pore volume and (c) pore size distribution of the Co_1/NC and Co_1/NC-h catalysts.
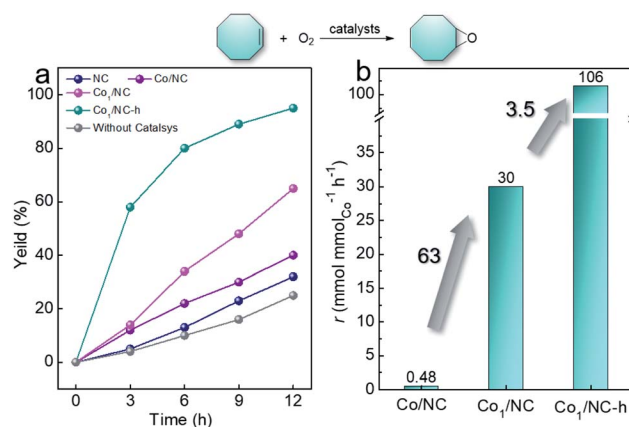
Fig. 3 Catalytic performance of cyclooctene epoxidation. (a) The time course of conversion of cyclooctene. (b) Catalytic reaction rate of various catalysts based on each Co atom. Reaction conditions: catalysts (5 mg), cyclooctene (0.5 mmol), DMF (2 mL), 140 °C and 0.5 MPa O_2.

6018 | J. Mater. Chem. A, 2022, 10, 6016–6022

This journal is © The Royal Society of Chemistry 2022

porous structure, the Co_1/NC-h catalysts yielded an excellent catalytic performance for cyclooctene epoxidation with O_2 as the oxidant.

Mechanism analysis

Initially, the single-atom Co was considered as the active site for cyclooctene epoxidation, which could be confirmed *via* removing the metal atoms in the Co_1/NC-h catalysts. At 80 °C, single-atom Co in Co_1/NC-h was etched with HNO_3 (5 mol L^{-1}) for 12 h. As shown in Fig. 4a, the reaction rate of cyclooctene epoxidation catalyzed by the HNO_3 treated Co_1/NC-h catalyst was only 0.006 mmol mL^{-1} h^{-1}, which was greatly lower than that catalyzed by fresh Co_1/NC-h (0.048 mmol mL^{-1} h^{-1}), but similar to the rate without catalysts (0.0052 mmol mL^{-1} h^{-1}). Therefore, the critical function of Co atoms in cyclooctene epoxidation was confirmed.

Except the intrinsically active Co atoms, the different environments of Co atoms could also result in totally distinct catalytic activity between Co/NC and Co_1/NC-h. As shown in Fig. S6† and 4b, the Co/NC catalysts exhibited a similar multiscale porous structure and defect of N-doped carbon to those of Co_1/NC-h. However, the different catalytic performance of two catalysts revealed that other factors such as the differences in the coordination mode of N atoms could play a crucial role. In previous reports, the Co–N_x active sites have been successfully confirmed in the single-atom Co-anchored on the N-doped carbon supports with the same carbonization process.[32,40] For the Co_1/NC-h catalysts, the Co–N_x active sites were detected from the XPS analysis of N 1s peaks (Fig. 4c). The corresponding valence state of Co atoms was +2 in the Co_1/NC-h catalysts (Fig. 4d). Although the Co–N_x active sites were also detected (Fig. 4c), the fraction of Co^0 was 27.4% from the XPS analysis of Co 2p in the fresh Co/NC catalysts (Fig. 4d). As shown in Fig. S7,† these metallic Co atoms could be easily oxidized along with the formation of a Co–O bond during the epoxidation of cyclooctene.

Therefore, the different fraction of Co–N_x active sites in Co_1/NC-h and Co/NC catalysts led to their different catalytic performance of cyclooctene epoxidation. The O_2 activation of the Co–N_x and Co–O active sites directly determined the intrinsic catalytic activity of Co_1/NC and Co/NC catalysts. To explore their intrinsic activity, DFT simulation was employed to verify the adsorption behavior of O_2 molecules and reactive oxygen atoms. As previously reported, a Co atom coordinated with three N atoms and one C atom (Co–N_3) was selected as the model local structure of single-atom Co_1/NC-h catalysts, as referenced from previous reports.[36,37] Meanwhile, the CoO surface was the model surface owing to the existence of Co^{2+} in the used Co/NC catalysts from the XPS analysis (Fig. S7†). As shown in Fig. 5a and S8a,† the Co–N_3 and CoO surfaces exhibited a similar adsorption strength for O_2, resulting in a similar degree of activation.

During the epoxidation process, the Co active sites could be occupied by O_2 molecules (Fig. 5a) to give a Co(III)OO• superoxo complex (**I**), as shown in Fig. S9.† The superoxo complex facilitates interaction with the double bond of the alkene and then undergoes a migratory insertion to form a cobalt peroxo complex (**II**), followed by the formation of a four membered cyclic radical intermediate (**III**).[19,20,41–44] Finally, the four membered cyclic radical intermediate reacts with another alkene molecule to give the epoxide product (Fig. S9†). Thus, the Co–O bond breaking will further affect the desorption of the cobalt peroxo complex to give the four membered cyclic radical
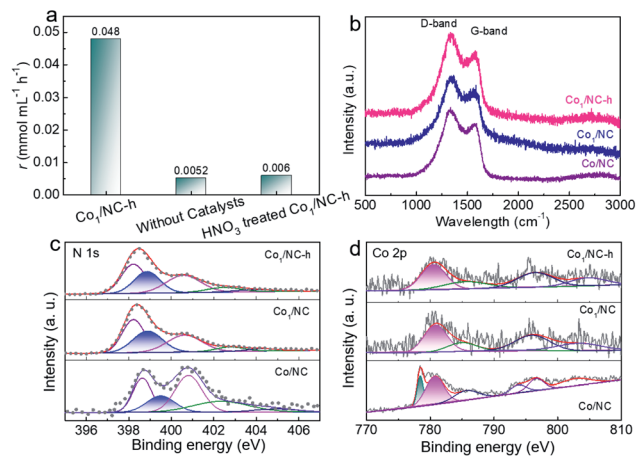
Fig. 4 (a) Reaction rate of various catalysts for cyclooctene epoxides. Reaction conditions: cyclooctene (0.5 mmol), catalysts (5 mg), DMF (2 mL), 140 °C and 0.5 MPa O_2. (b) Raman spectral analysis of the Co_1/NC-h, Co_1/NC and Co/NC catalysts. XPS analysis of (c) N 1s and (d) Co 2p peaks of the Co_1/NC-h, Co_1/NC and Co/NC catalysts.
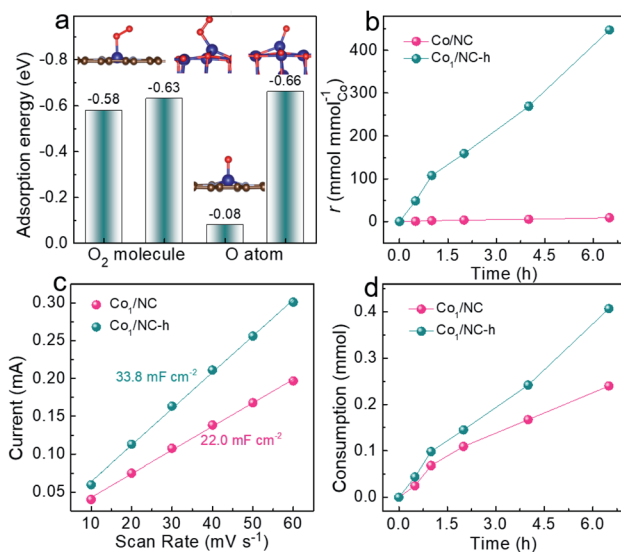
Fig. 5 (a) Adsorption behavior of the O_2 molecule and O atom on the Co–N_3 and CoO surfaces. Red: O atom, dark blue: Co atom, and dark brown: C atom. (b) The consumption rate of 3,5-di-*tert*-butyl-4-hydroxytoluene based on Co atoms catalyzed by the Co_1/NC-h and Co/NC catalysts. Reaction conditions: 3,5-di-*tert*-butyl-4-hydroxytoluene (1 mmol), catalysts (5 mg), DMF (2 mL), 80 °C and 1 MPa O_2. (c) Current as a function of scan rate. (d) The consumption rate of 3,5-di-*tert*-butyl-4-hydroxytoluene based on Co atoms catalyzed by the Co_1/NC-h and Co_1/NC catalysts. Reaction conditions: 3,5-di-*tert*-butyl-4-hydroxytoluene (1 mmol), catalysts (5 mg), DMF (2 mL), 80 °C and 1 MPa O_2.

This journal is © The Royal Society of Chemistry 2022

J. Mater. Chem. A, 2022, **10**, 6016–6022 | **6019**

intermediate. Due to their different coordination environments, the O atom exhibited greatly stronger adsorption on the CoO surface than on the Co–N$_3$ active sites (Fig. 5a and S8b†). Therefore, the weak interaction between the O atom and single-atom Co further improves the desorption of the cobalt peroxo complex, while the strong adsorption of the reactive O atom on CoO leads to weak activity for epoxidation.

Meanwhile, 3,5-di-*tert*-butyl-4-hydroxytoluene was selected as the model molecule to investigate the generation of reactive oxygen species. As shown in Fig. 5b, the consumption rate of 3,5-di-*tert*-butyl-4-hydroxytoluene was 107.7 mmol mmol$_{Co}^{-1}$ h^{-1} for the single-atom Co$_1$/NC-h catalysts, while only a 1.4 mmol mmol$_{Co}^{-1}$ h^{-1} consumption rate was obtained with the Co/NC catalysts under the same reaction conditions. The huge gap between Co$_1$/NC-h and Co/NC showed that the Co–N$_x$ active sites could generate a larger number of reactive oxygen species compared with Co–O. Thus, the intrinsic catalytic activity of Co–N$_x$ sites was demonstrated by combining DFT simulation with the consumption rate of 3,5-di-*tert*-butyl-4-hydroxytoluene.

Then, the influence of the multiscale porous structure on the catalytic activity could be obtained by comparing the reaction rate of Co$_1$/NC and Co$_1$/NC-h catalysts. The same structural features of carbon supports and the same coordinated environment as well as the same Co valence revealed that the Co$_1$/NC and Co$_1$/NC-h catalysts exhibited the same Co–N$_x$ active sites for cyclooctene epoxidation (Fig. 4b–d). However, due to the multiscale porous structure, Co$_1$/NC-h can expose more accessible active sites for reactants, resulting in the increase of overall catalytic activity. The exposed number of active sites could be correlated with the electrochemically active surface area, which was investigated by measuring the electrochemical double-layer capacitance (C_{dl}). The C_{dl} was obtained through cyclic voltammetric curves recorded at various scan rates from 10 to 60 mV s^{-1} (Fig. S10†). As shown in Fig. 5c, the C_{dl} value of Co$_1$/NC-h catalysts was calculated to be 33.8 mF cm^{-2}, which was 1.5 times higher than that of Co$_1$/NC catalysts (22.0 mF cm^{-2}). Therefore, the enhanced C_{dl} value indicated that more active sites were exposed on Co$_1$/NC-h catalysts.

Meanwhile, the consumption of 3,5-di-*tert*-butyl-4-hydroxytoluene was also determined to further verify the difference in the number of exposed Co–N$_x$ active sites in the Co$_1$/NC-h and Co$_1$/NC catalysts. With the same total number of Co–N$_x$ active sites, the consumption rate of 3,5-di-*tert*-butyl-4-hydroxytoluene on Co$_1$/NC-h was 0.063 mmol h^{-1}, which was 1.7 times higher than 0.037 mmol h^{-1} obtained when catalyzed by Co$_1$/NC. The improved consumption rate of Co$_1$/NC-h also proved that more Co–N$_x$ active sites were involved in the catalytic reaction, consistent with the electrochemically active surface areas of the two catalysts as shown in Fig. 5c.

Based on the above analysis, the single atom Co active sites in N-doped carbon supports exhibited a high intrinsic activity for O$_2$ activation. Meanwhile, the multiscale porous structure in the catalysts resulted in the increase of the available number of exposed active sites for catalysis. Therefore, it is not surprising that Co$_1$/NC-h with single-atom Co and a multiscale porous
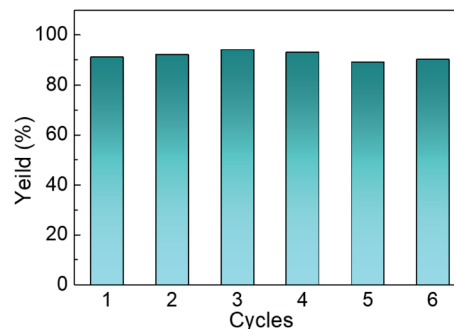

Fig. 6 Catalytic stability of the Co$_1$/NC-h catalysts for cyclooctene epoxidation. Reaction conditions: cyclooctene (0.5 mmol), catalysts (5 mg), DMF (2 mL), 140 °C, 0.5 MPa O$_2$ and 9 h reaction.

structure exhibited excellent catalytic performance for cyclooctene epoxidation.

In addition, catalytic stability is also a critical factor to evaluate the catalytic performance of the present catalysts. After the reaction, the Co$_1$/NC-h catalysts could be easily recycled by centrifugation and reused for the next cycles without any treatment. As shown in Fig. 6, the final yield of 1,2-epoxycycloheptane was maintained in the range of 89%~94% without an obvious decrease for 6 cycles. The morphology of the used Co$_1$/NC-h catalysts was well preserved during the recycling process (Fig. S11a†). Meanwhile, there was no metallic Co and/or cobalt oxide phases in the spent Co$_1$/NC-h catalysts, as revealed by the XRD pattern (Fig. S11b†). The XPS analysis of the Co 2p peak on the fresh and used Co$_1$/NC-h catalysts also suggested the preserved electronic structure of Co in the catalysts after catalytic reactions (Fig. S11c†). Determined by ICP-MS, the Co ions were not detected in the reaction solution. Taking all together, the un-degraded catalytic activity as well as the unchanged morphological features of the Co$_1$/NC-h catalysts demonstrated the excellent catalytic stability of the catalysts.

Conclusions

In summary, multiscale porous Co$_1$/NC-h catalysts have been successfully constructed by etching CoZn-ZIF precursors before a carbonation process. Owing to the improved utilization of active Co–N$_x$ sites with high intrinsic activity and the exposure of more active sites when the number of macropores increased and the number of micropores decreased, the Co$_1$/NC-h catalysts exhibit an exceptional catalytic activity for cyclooctene epoxidation with O$_2$ as the oxidant. The results presented in this work could guide the rational design and synthesis of prominent single-atom catalysts for both basic research and practical applications.

Experimental section

Chemicals and materials

All of the starting reagents for the synthesis and reactions were commercially available and were used as received. Zinc(ɪɪ) nitrate hexahydrate (Zn(NO$_3$)$_2$·6H$_2$O, Energy Chemical, 99%),

6020 | *J. Mater. Chem. A*, 2022, **10**, 6016–6022

This journal is © The Royal Society of Chemistry 2022

cobalt(II) nitrate hexahydrate ($Co(NO_3)_2 \cdot 6H_2O$, Energy Chemical, 98%), 2-methylimidazole (2-MeIM, Energy Chemical, 98%), cyclooctene (Energy Chemical, 95%), methanol (Energy Chemical, 99.9%), DMF (N,N-dimethylformamide, Sigma Aldrich, 99.8%, with molecular sieves), and 3,5-di-*tert*-butyl-4-hydroxytoluene (Energy Chemical, 99%).

Materials preparation

Preparation of CoZn-ZIF, Co-ZIF, and Zn-ZIF. The preparation methods of CoZn-ZIF were prepared by following reported procedures.[40] In a typical synthesis, a mixture of $Co(NO_3)_2 \cdot 6H_2O$ (3.75 mmol) and $Zn(NO_3)_2 \cdot 6H_2O$ (3.75 mmol) was dissolved in 30 mL methanol (solution 1) and 2-MeIM (15 mmol) was dissolved in 30 mL methanol (solution 2). After forming a homogeneous solution, solution 1 was slowly added into solution 2 under stirring, and the final mixture was stirred constantly at 30 °C for 6 h to form CoZn-ZIF. The obtained product was collected by centrifugation, followed by washing with methanol for 3 times and drying at 60 °C in an oven.

Co-ZIF and Zn-ZIF were synthesized following the same preparation procedures by using a single metal salt of $Co(NO_3)_2 \cdot 6H_2O$ (3.75 mmol) and $Zn(NO_3) \cdot 6H_2O$ (3.75 mmol), respectively.

Preparation of CoZn-ZIF-h. In a typical synthesis, 250 mg of CoZn-ZIF was dispersed into 50 mL DMF solvent under ultrasound to form a uniform mixture. Then, the mixture was heated up to 140 °C and hold for 24 h under an air atmosphere with constant stirring. After the etching procedure, the obtained CoZn-ZIF-h was collected by centrifugation, followed by washing with methanol for 3 times and drying at 60 °C in an oven.

Preparation of Co$_1$/NC-h, Co$_1$/NC, Co/NC and NC. The Co$_1$/NC-h catalysts were prepared *via* the carbonization of CoZn-ZIF-h. In the process, 300 mg of CoZn-ZIF-h was placed in a tube furnace, which was flushed with N_2 gas at a speed of 80 sccm to remove air before heating. Then, the sample was heated to 900 °C at a rate of 5 °C min^{-1} and the temperature was maintained at 900 °C for 2 h under N_2. Finally, it was naturally cooled to room temperature and the Co$_1$/NC-h catalyst was obtained.

The Co$_1$/NC, Co/NC and NC catalysts were obtained by the pyrolysis of CoZn-ZIF, Co-ZIF and Zn-ZIF at 900 °C for 2 h under N_2 with the same process, respectively.

Preparation of HNO$_3$ etched Co$_1$/NC-h. In the process, 50 mg of Co$_1$/NC-h catalyst was dispersed into 30 mL of 5 mol L^{-1} HNO$_3$ aqueous solution, and then the mixture was heated to 80 °C and hold for 12 h with reflux condensation under stirring. After that, the solution was cooled to room temperature, and the separated solid was washed with deionized water several times until the solution was neutral. Finally, the obtained HNO$_3$ etched Co$_1$/NC-h sample was collected by centrifugation and drying at 60 °C in an oven.

Characterization methods

The structures of the obtained ZIFs and carbon materials were characterized by X-ray power diffraction (XRD) using a Shimadzu XRD-6000 with Cu Kα radiation. Field-emission scanning electron microscopy (FE-SEM, FEI Verios G4) and transmission electron microscopy (TEM, FEI Talos F200X TEM) with an accelerating voltage of 200 kV were performed to analyze the morphology of samples. HAADF-STEM images and EDS mappings of samples were obtained using a double Cs corrector transmission electron microscope (FEI Themis Z). The Co content of samples was identified by inductively coupled plasma mass spectrometry (ICP-MS, PerkinElmer NexION 350D ICP-MS). The valence state of samples was monitored by X-ray photoelectron spectroscopy (XPS, Thermo Fisher Scientific ESCALAB Xi+) with a monochromatic Al Kα line. The Brunauer–Emmett–Teller (BET) specific surface areas of catalysts were measured from the nitrogen adsorption–desorption isotherms at 77 K (Bei Shi De Instrument 3H-2000PS2). The Raman spectrum of samples was collected using a Raman spectrometer (Horiba JOBIN YVON) with a 633 nm laser device.

Catalyst evaluation

General procedure. All reactions were performed in a stainless-steel autoclave. In a typical catalytic epoxidation reaction of cyclooctene, 0.5 mmol of cyclooctene and 5 mg of catalysts were mixed in 2 mL DMF. Then, the mixture was transferred to the autoclave charged with 0.5 MPa O_2 pressure at 140 °C with stirring. After the reaction, the mixture was cooled to room temperature and the catalyst was filtered off. Then the mixture was diluted with methanol and analyzed by gas chromatography (Agilent 7890) using a flame ionization detector (FID) and GC-MS (Agilent 7890 GC and 5975C MSD) with m-xylene as the internal standard. The reaction mixture was taken at different time intervals for analysis.

The performance of reaction active oxygen species generation of Co/NC, Co$_1$/NC-h and Co$_1$/NC catalysts. 1 mmol of 3,5-di-*tert*-butyl-4-hydroxytoluene and 5 mg of catalysts were mixed in 2 mL DMF. The mixture was transferred to the autoclave charged with 1 MPa O_2 pressure at 80 °C with stirring. After the reaction, the self-coupling products were analyzed by GC (Agilent 7890) with *m*-xylene as the internal standard.

Stability tests. A mixture of 0.5 mmol of cyclooctene, 5 mg of Co$_1$/NC-h catalyst and 2 mL of DMF was added to the autoclave. The reaction mixture was heated to 140 °C under stirring and charged with 0.5 MPa O_2. After 9 h of reaction, the mixture was cooled to room temperature and the catalyst was filtered off. Then the mixture was analyzed by GC7890. The filtered catalyst was collected and re-dispersed into a new reaction mixture and continued the reaction under the same reaction conditions.

Conflicts of interest

There are no conflicts to declare.

Acknowledgements

This journal is © The Royal Society of Chemistry 2022

J. Mater. Chem. A, 2022, **10**, 6016–6022 | **6021**

Notes and references

1 J. He, J. Ling and P. Chiu, *Chem. Rev.*, 2014, **114**, 8037–8128.
2 R. L. Davis, J. Stiller, T. Naicker, H. Jiang and K. A. Jorgensen, *Angew. Chem., Int. Ed.*, 2014, **53**, 7406–7426.
3 B. S. Lane and K. Burgess, *Chem. Rev.*, 2003, **103**, 2457–2473.
4 D. T. Bregante, M. C. Chan, J. Z. Tan, E. Z. Ayla, C. P. Nicholas, D. Shukla and D. W. Flaherty, *Nat. Catal.*, 2021, **4**, 797–808.
5 C. Miao, B. Wang, Y. Wang, C. Xia, Y.-M. Lee, W. Nam and W. Sun, *J. Am. Chem. Soc.*, 2016, **138**, 936–943.
6 N. A. Grosso-Giordano, C. Schroeder, A. Okrut, A. Solovyov, C. Schottle, W. Chasse, N. Marinkovic, H. Koller, S. I. Zones and A. Katz, *J. Am. Chem. Soc.*, 2018, **140**, 4956–4960.
7 D. T. Bregante, A. M. Johnson, A. Y. Patel, E. Z. Ayla, M. J. Cordon, B. C. Bukowski, J. Greeley, R. Gounder and D. W. Flaherty, *J. Am. Chem. Soc.*, 2019, **141**, 7302–7319.
8 C. Ehinger, C. P. Gordon and C. Coperet, *Chem. Sci.*, 2019, **10**, 1786–1795.
9 X. Engelmann, D. D. Malik, T. Corona, K. Warm, E. R. Farquhar, M. Swart, W. Nam and K. Ray, *Angew. Chem., Int. Ed.*, 2019, **58**, 4012–4016.
10 M. Zhang, V. Singh, X. Hu, X. Ma, J. Lu, C. Zhang, J. Wang and J. Niu, *ACS Catal.*, 2019, **9**, 7641–7650.
11 J. Teržan, M. Huš, B. Likozar and P. Djinović, *ACS Catal.*, 2020, **10**, 13415–13436.
12 A. S. Sharma, V. S. Sharma, H. Kaur and R. S. Varma, *Green Chem.*, 2020, **22**, 5902–5936.
13 K. Schroder, B. Join, A. J. Amali, K. Junge, X. Ribas, M. Costas and M. Beller, *Angew. Chem., Int. Ed.*, 2011, **50**, 1425–1429.
14 Y. Nishiyama, Y. Nakagawa and N. Mizuno, *Angew. Chem., Int. Ed.*, 2001, **40**, 3639–3641.
15 R. Neumann and M. Dahan, *Nature*, 1997, **388**, 353–355.
16 D. Shabashov and M. P. Doyle, *Tetrahedron*, 2013, **69**, 10009–10013.
17 P. Mekrattanachai, J. Liu, Z. Li, C. Cao and W. Song, *Chem. Commun.*, 2018, **54**, 1433–1436.
18 S. Tian, Q. Fu, W. Chen, Q. Feng, Z. Chen, J. Zhang, W. C. Cheong, R. Yu, L. Gu, J. Dong, J. Luo, C. Chen, Q. Peng, C. Draxl, D. Wang and Y. Li, *Nat. Commun.*, 2018, **9**, 2353.
19 C. Weerakkody, S. Biswas, W. Song, J. He, N. Wasalathanthri, S. Dissanayake, D. A. Kriz, B. Dutta and S. L. Suib, *Appl. Catal., B*, 2018, **221**, 681–690.
20 L. Qian, Z. Wang, E. V. Beletskiy, J. Liu, H. J. Dos Santos, T. Li, M. D. Rangel, M. C. Kung and H. H. Kung, *Nat. Commun.*, 2017, **8**, 14881.
21 Y. Xiaofeng, W. Aiqin, Q. Botao, L. Jun, L. Jinyue and Z. Tao, *Acc. Chem. Res.*, 2016, **46**, 1740–1748.
22 H. Yan, C. Su, J. He and W. Chen, *J. Mater. Chem. A*, 2018, **6**, 8793–8814.
23 M. B. Gawande, P. Fornasiero and R. Zbořil, *ACS Catal.*, 2020, **10**, 2231–2259.
24 Y. Shang, X. Xu, B. Gao, S. Wang and X. Duan, *Chem. Soc. Rev.*, 2021, **50**, 5281–5322.
25 Q. Ren, H. Wang, X. F. Lu, Y. X. Tong and G. R. Li, *Adv. Sci.*, 2018, **5**, 1700515.
26 H. Zhang, X. F. Lu, Z. P. Wu and X. W. D. Lou, *ACS Cent. Sci.*, 2020, **6**, 1288–1301.
27 B. Q. Li, C. X. Zhao, J. N. Liu and Q. Zhang, *Adv. Mater.*, 2019, **31**, 1808173.
28 C. Tang, B. Wang, H. F. Wang and Q. Zhang, *Adv. Mater.*, 2017, **29**, 1703185.
29 C. Wan, X. Duan and Y. Huang, *Adv. Energy Mater.*, 2020, **10**, 1903815.
30 Y. Hu, H. Li, Z. Li, B. Li, S. Wang, Y. Yao and C. Yu, *Green Chem.*, 2021, **23**, 8754–8794.
31 Y. Zhao, H. Zhou, W. Chen, Y. Tong, C. Zhao, Y. Lin, Z. Jiang, Q. Zhang, Z. Xue, W. C. Cheong, B. Jin, F. Zhou, W. Wang, M. Chen, X. Hong, J. Dong, S. Wei, Y. Li and Y. Wu, *J. Am. Chem. Soc.*, 2019, **141**, 10590–10594.
32 X. Wang, W. Chen, L. Zhang, T. Yao, W. Liu, Y. Lin, H. Ju, J. Dong, L. Zheng, W. Yan, X. Zheng, Z. Li, X. Wang, J. Yang, D. He, Y. Wang, Z. Deng, Y. Wu and Y. Li, *J. Am. Chem. Soc.*, 2017, **139**, 9419–9422.
33 X. F. Lu, Y. Fang, D. Luan and X. W. D. Lou, *Nano Lett.*, 2021, **21**, 1555–1565.
34 D. Malko, A. Kucernak and T. Lopes, *Nat. Commun.*, 2016, **7**, 13285.
35 J. Liu, Z. Gong, C. Allen, W. Ge, H. Gong, J. Liao, J. Liu, K. Huang, M. Yan, R. Liu, G. He, J. Dong, G. Ye and H. Fei, *Chem Catalysis*, 2021, **1**, 1–17.
36 C. Zhao, X. Dai, T. Yao, W. Chen, X. Wang, J. Wang, J. Yang, S. Wei, Y. Wu and Y. Li, *J. Am. Chem. Soc.*, 2017, **139**, 8078–8081.
37 S. Lai, L. Xu, H. Liu, S. Chen, R. Cai, L. Zhang, W. Theis, J. Sun, D. Yang and X. Zhao, *J. Mater. Chem. A*, 2019, **7**, 21884–21891.
38 H. Yang, L. Shang, Q. Zhang, R. Shi, G. I. N. Waterhouse, L. Gu and T. Zhang, *Nat. Commun.*, 2019, **10**, 4585.
39 X. Li, A. E. Surkus, J. Rabeah, M. Anwar, S. Dastigir, H. Junge, A. Bruckner and M. Beller, *Angew. Chem., Int. Ed.*, 2020, **59**, 15849–15854.
40 J. Yang, F. Zhang, H. Lu, X. Hong, H. Jiang, Y. Wu and Y. Li, *Angew. Chem., Int. Ed.*, 2015, **54**, 10889–10893.
41 J. Sebastian, K. Jinka and R. Jasra, *J. Catal.*, 2006, **244**, 208–218.
42 Q. Tang, Q. Zhang, H. Wu and Y. Wang, *J. Catal.*, 2005, **230**, 384–397.
43 A. Peng, M. C. Kung, R. R. O. Brydon, M. O. Ross, L. Qian, L. J. Broadbelt and H. H. Kung, *Sci. Adv.*, 2020, **6**, eaax6637.
44 C. P. Gordon, H. Engler, A. S. Tragl, M. Plodinec, T. Lunkenbein, A. Berkessel, J. H. Teles, A.-N. Parvulescu and C. Copéret, *Nature*, 2020, **586**, 708–713.